frontiers | Frontiers in Materials

TYPE Original Research
PUBLISHED 04 February 2025
DOI 10.3389/fmats.2025.1527502

OPEN ACCESS

EDITED BY
Jialai Wang,
University of Alabama, United States

REVIEWED BY
Mahmoud Ebrahimi,
University of Maragheh, Iran
Amir Ali Shahmansouri,
Washington State University, United States

*CORRESPONDENCE
Zheng Chen,
chenzheng@gxu.edu.cn

RECEIVED 13 November 2024
ACCEPTED 13 January 2025
PUBLISHED 04 February 2025

CITATION
Li X, Jiang G, Wang N, Wei Y, Chen Z, Li J, Chen B and Yu J (2025) Study of interfacial bonding properties and shrinkage deformation of cement-alkali activated gradient-structured composite in complex environments with temperature-humidity changes.
Front. Mater. 12:1527502.
doi: 10.3389/fmats.2025.1527502

Study of interfacial bonding properties and shrinkage deformation of cement-alkali activated gradient-structured composite in complex environments with temperature-humidity changes

Xinzhe Li[1], Ganyou Jiang[2], Naishuang Wang[1], Yisong Wei[1], Zheng Chen[3,4]*, Jing Li[3,4], Ben Chen[3,4] and Jiamin Yu[3,4]

[1]Guangxi Road and Bridge Engineering Group Co, Nanning, China, [2]Guangxi Guanglu Industrial Investment Group Co, Nanning, China, [3]Key Laboratory of Disaster Prevention and Structural Safety of Ministry of Education, Guangxi University, Nanning, China, [4]School of Civil Engineering and Architecture, Guangxi University, Nanning, China

The early shrinkage-deformation and mechanical property evolution of gradient-structured composites in extreme environments are still insufficient. The paper prepared ordinary Portland cement-alkali-activated slag (OPC-AAS) and ordinary Portland cement-alkali-activated metakaolin (OPC-AAMK) gradient-structured composite by stacking cement and alkali-activated materials together. The effects of temperature difference cycling and wetdry cycling extremes on the early shrinkage strain and splitting strength of OPC-AAS and OPC-AAMK composites, as well as the structure of the bond interface and the micromorphology of the hydration products, were comparatively analyzed. The results demonstrated that the temperature difference cycling affected the early deformation and bond strength of the gradient-structured composite interfaces more significantly than the dry-wet cycling. The maximum expansion strains of OPC-AAS and OPC-AAMK were 1,130.88 μm and 1,399.25 μm, respectively, under the effect of temperature difference cycling; the splitting strengths of OPC-AAS and OPC-AAMK after three cycles of temperature difference cycling were reduced by 26.37% and 31.32%, respectively, compared with that after three cycles of wet-dry cycling. In addition, the OPC-AAS composites showed better interfacial bonding properties after extreme environmental cycling compared to the OPC-AAMK composites. The early splitting strengths under the two extreme environmental effects increased and then decreased, and the maximum splitting strengths of OPCAAS were 2.66 MPa and 3.65 MPa under the temperature difference cycling and dry-wet cycling, respectively, which were 5.14% and 35.69% higher than those of OPC-AAMK, respectively. Scanning electron microscopy (SEM) characterization analysis showed that the temperature difference cycling resulted in more severe product decomposition of the AAMK cementitious material, and obvious cracks and holes appeared at the bonding interface of OPC-AAMK. This study provides some references for the optimal design of the early

shrinkage-deformation properties and mechanical properties of gradient-structured composites under extreme environments as well as the assessment of service life.

KEYWORDS

gradient-structured composite, alkali-activated mortar, temperature difference cycling, wet-dry cycling, shrinkage strain, splitting strength

Highlights

- The effects of temperature difference cycling and dry-wet cycling effects on the early shrinkage and deformation of gradient-structured composite were investigated.
- The effects of interfacial bonding properties and splitting strength of gradient-structured composite under extreme conditions were explored.
- Comparatively analyzed the influence of different gradient-structured composite by temperature difference cycling and dry-wet cycling.

1 Introduction

Concrete materials have the advantages of easy access to materials, high compressive strength, good compatibility, good moldability, and good combination with reinforcement and fibers and other reinforcements. They are widely used in municipal bridges, high-speed railways, ports, terminals, and other infrastructures, where cement is the main ingredient of concrete. It is also the most widely used cementitious material in constructing modern infrastructures (Othman et al., 2016; Meng et al., 2024; Ikumi et al., 2016). However, due to the characteristics of concrete itself, such as low tensile strength, poor crack resistance, brittleness, poor thermal insulation, self-weight, single function, etc., to a large extent, limiting the scope of its application, and the generation of cement released by the CO_2 subconsciously change the human living environment.

With the development of society, people's awareness of protecting the natural ecological environment has been gradually enhanced. The concepts of planted concrete (Liu et al., 2024a) and alkali activated concrete (Torelli et al., 2020; Liu et al., 2024b; Dai et al., 2024) have been proposed accordingly. Above all, alkali-activated concrete is an innovative, low-carbon and green building material that represents a promising new avenue for advancing sustainability in civil engineering (Benito et al., 2013). Compared to traditional Portland cement, alkali activated concrete requires only 41% of energy consumption and emits 20% of CO_2 per ton. In addition, if industrial by-products such as slag, gangue or fly ash are utilized in the production of alkali activated concrete, carbon emissions and energy consumption can be further reduced (Davidovits, 2018). However, there are problems such as large shrinkage, easy to crack and so on, which limits the popularization and application of alkali-activated concrete (Gao et al., 2020; Matalkah et al., 2019). Especially with the increase in the level of ultra-high-rise, mega-span and intelligent buildings, the traditional cement-based concrete materials prepared using a single, uniform pouring method are increasingly showing their unsuitability. Therefore, many scholars have long been exploring methods and approaches to improve the performance of concrete and enhance the mechanical properties and service durability under extreme environments. The application of gradient structure concrete can effectively improve the comprehensive performance of cementitious materials, solve the problems of weaker interface, single function, lower tensile strength, and poor toughness (Yang Jiujun et al., 2001), and can extend the applicability of concrete in complex special engineering environments. Therefore, the application of functional gradient structure in the field of cement concrete materials has also attracted the attention of more and more researchers, making

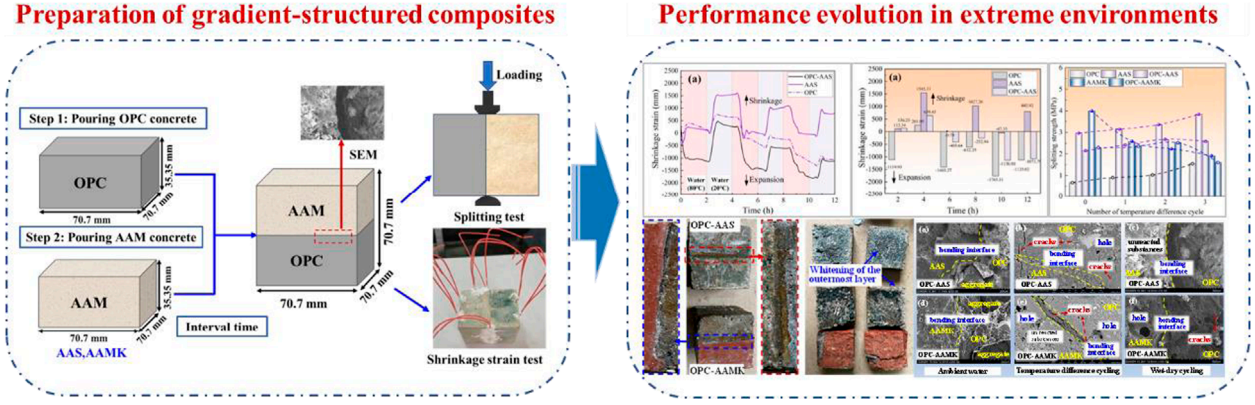

GRAPHICAL ABSTRACT

functional gradient concrete an important branch in structural engineering (Wang et al., 2020).

In recent years, there are many reports on the use of gradient composite to solve the problems of weak interface, poor toughness, low tensile strength and single function of cementitious materials (Yang Jiujun et al., 2001; Jiu-Jun et al., 2003; Qilong Li Birong and Guoliang, 1999; Ma et al., 2006; Qinghua and Shilong, 2009; Zhi-Hua et al., 2016; Wen et al., 2010; Wörner et al., 2016). Fang et al. (2013) prepared functional gradient concrete beams using ECC and normal concrete, and conducted experimental studies on the flexural properties of functional gradient concrete beams. The test results showed that during ultimate damage, localized debonding of layer boundaries would occur at the roots of individual cracks in some specimens, but it would not lead to serious stripping of the ECC layer from the concrete layer. It can be seen that the functional gradient concrete has a weak discontinuous zone at the interface between the ECC layer and the ordinary concrete layer, and the performance of its interlayer interface has an important influence on the bending damage pattern of the beam. ZiYu (2023) used Decorative Ultra High Performance Concrete (DUHPC) compounded with normal concrete (NC) to form gradient concrete. The effects of the gradient concrete casting time interval and strength on the bond performance of gradient concrete were investigated. The results show that with the shortening of the casting time interval and the reduction of the strength difference, the bonding performance of gradient concrete increases, and the more obvious the interfacial transition zone at the bond, the better the bonding performance. In addition, other scholars have investigated the effect of pores and their distribution at the interface on the interlayer strength (He et al., 2024a) and interlayer stress (He et al., 2024b) by 3D printing concrete technology. There has been much attention paid to the shrinkage-deformation and interfacial properties of cementitious composites. Chen et al. investigated the spatio-temporal autogenous shrinkage and cracking behavior of core concrete in full-scale CFST (Chen et al., 2024a), while also exploring innovative strategies for cement paste flowability control (Chen et al., 2024b). The mechanical properties and durability of composites under complex environments have been extensively studied, with research examining the chlorine resistance of concrete based on pouring interval time (Chen et al., 2024c) and the residual impact resistance of PVA fiber reinforced cement mortar after chloride erosion (Chen et al., 2024d). Furthermore, studies on the behavior of steel-reinforced recycled aggregate concrete-filled GFRP tubular columns (Tang et al., 2024) and the corrosion resistance of geopolymer concrete with BFRP bars in seawater (Chen et al., 2023) have provided valuable insights into composite performance under extreme conditions. Advanced detection methods, including 3D vision technologies and structural damage recognition robots (Li et al., 2024), as well as dual-frequency lidar systems for compressed sensing 3D imaging (Hu et al., 2024), have significantly enhanced the accuracy and efficiency of composite material analysis and monitoring (Jamal Jumaah et al., 2024).

In conclusion, for gradient-structured composite, the bonding performance of the interface is crucial to ensure the reliability of the structure, and if the interfacial bonding of the gradient-structured composite is not effective, it will lead to weaker bond strength and greater interfacial permeability, which is not favorable to the durability of the structure (Jun et al., 2019; Panda et al., 2019). Most of the studies have also shown that a variety of factors such as concrete rheological properties, interlayer casting time interval, etc. affect the interlayer bond of multilayer cast concrete (Latif Baloch et al., 2021; Xu et al., 2021; Keita et al., 2019; Dybeł and Kucharska, 2020; Navarrete et al., 2021), but no study has shown the effect of different service environment changes on the early interfacial bond strength and expansion and contraction properties of composites. It is well known that in the hot summer, during the day, the temperature of the structural surface itself is often higher than the environmental temperature, generally up to 60°C or more, and at night the temperature of the structural surface will be drastically reduced to the ambient temperature, which will form a large temperature difference cyclic effect at the bond interface, which will easily lead to the debonding of the bond interface of the specimen and its failure (Chen et al., 2021). Similarly, for the marine concrete buildings in the tidal splash zone, due to the alternating wet and dry effects are often eroded to a very serious degree (Ting et al., 2021).

Based on this, for the defects of gradient-structured composites in service under the above extreme environments, this study set up deformation monitoring and mechanical tests under three environments (ambient water, temperature difference cycling, and dry- wet cycling) using gradient-structured composites OPC-AAS and OPC-AAMK as test objects. The early shrinkage properties of the gradient structural composites in extreme environments and the early splitting strength at the bond interface were investigated, and the corrosion morphology of the composites in different extreme environments was analyzed by scanning electron microscopy (SEM) method. The results of the study provide some reference for the optimized design of the early shrinkage and deformation properties and mechanical properties of the gradient structure composites under extreme environments, as well as the accurate assessment of the service life of the composites.

2 Experimental study

2.1 Materials and specimen preparations

P·II 42.5 R ordinary Portland cement (OPC) conforming to GB175-200 specifications was used in this paper. Slag that meets the GB/T 18046-2017 specification requirements is used. Metakaolin meets the GB175-200 specification. The mass and specific surface area of the raw materials and the compositional content of each element obtained by elemental analysis with an X-ray fluorescence spectroscopy (XRF) instrument are listed in Table 1. Standard sand conforms to GB/T-17671 specification, and its grain size ranges from 0.08 to 2 mm. The use of boric acid as a retarder (H_3BO_3, content ≥99.5%) is in line with GB/T 628-2011 specifications. Tap water was used as the mixing water in this study. In addition, a composite alkaline exciter made of water glass solution (27.30% SiO_2, 8.54% Na_2O, and 64.16% H_2O by mass) mixed with sodium hydroxide reagent (NaOH, ≥96.0%) was used as the alkaline exciter to stimulate the activity of slag or metakaolin.

The ordinary Portland cement and alkali-activated composite mixtures are listed in Table 2. Composite containing ordinary

TABLE 1 Chemical composition of cement, slag, and metakaolin.

Composition (wt%)	SiO_2	Al_2O_3	CaO	Fe_2O_3	MgO	Na_2O	K_2O	TiO_2	P_2O_5	LOI
Cement	20.7	5.12	60.4	5.44	0.83	0.23	0.27	1.24	<0.01	5.83
Slag	30.5	15.1	39.3	0.41	10.3	0.41	0.38	0.55	<0.01	3.05
Metakaolin	47.6	45.9	0.49	2.93	0.16	0.00	0.33	2.00	0.15	0.44

Note: LOI (Loss on ignition) in the table represents the measured loss on ignition of its components.

TABLE 2 Mixing ratios of ordinary Portland cement and alkali-activated composites.

Categories	Binder	Amount of binder/g	Sand/g	Alkaline activator/g	Water/g	Retarder/g
OPC	Cement	450	1,350	0	225	0
AAS	Slag	450	1,350	270.98 (Ms 1.5)	64.35	22.5
AAMK	Metakaolin	450	1,350	639.5 (Ms 1.2)	0.02	0

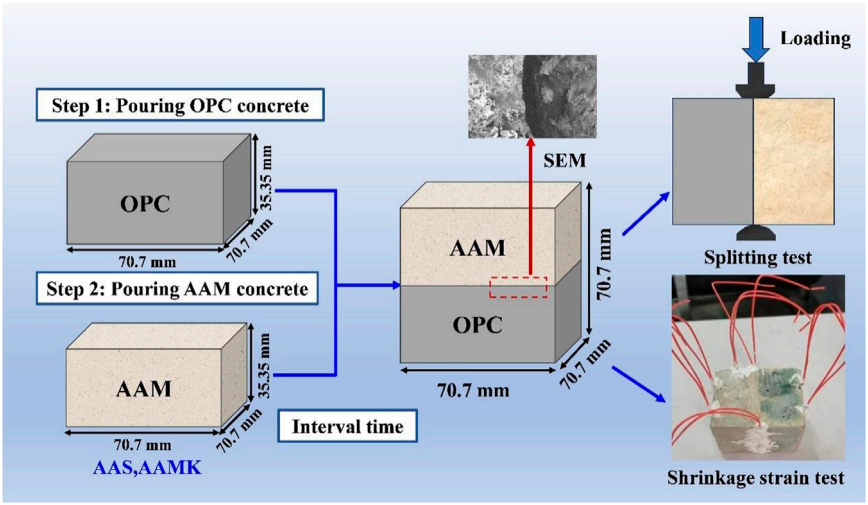

FIGURE 1
Schematic diagram of the layered casting of gradient-structured composite of OPC and AAS/AAMK.

Portland cement (OPC) and alkali-activated geopolymer (AAS/AAMK) was prepared using a two-step method based on the mixing ratios designed in Table 2. The composite specimens were made of cubic specimens with a side length of 70.7 mm, and the thickness of the OPC layer and the alkali-activated slag (AAS) and alkali-activated Metakaolin (AAMK) layer at half the depth of the mould, i.e., 35.35 mm per layer. As shown in Figure 1, fresh OPC was first poured into the mould, seal and curing for 12 h as an interval time, and then alkali-activated geopolymer concrete was cast into the mold as an overlay. The cast OPC-AAS and OPC-AAMK composites were wrapped with plastic sheeting, demoulded after 24 h, and the specimens were moved to a standard curing room (20°C, 95% RH) for 3 days. Expansion and shrinkage strain and splitting strength tests were carried out in different service environments.

2.2 Exposure conditions

The service environments were categorized as ambient water, temperature difference cycling and wet-dry cycling. For each environment, OPC-AAS composite and OPC-AAMK composite were prepared. The specific settings of the environmental parameters are shown in Table 3, and the composite was placed under these three environments for service for 12 h to observe the expansion and shrinkage changes. In the operation of the temperature difference cycling program, we used a heater to achieve a rapid rising of ambient water to 80°C, immersion to a specified time (2 h) and then switch to ambient water to achieve a rapid cooling to 20°C and immersion for 2 h. In this cycle, the high temperature in the water bath is set at 80°C and the low temperature is set at 20°C; In addition, for the operation of the wet-dry cycling program, in order to speed

TABLE 3 Design of service environments for cement-alkali activated gradient-structured composite.

Sample number	Service environment	Environmental conditions
OPC-AAS	Ambient water	Immersion in water at 20°C
	Temperature difference cycling	Immersion in water at 20°C for 2 h and at 80°C for 2 h
	Dry-wet cycling	Immersion in water at 20°C for 2 h and drying at 80°C for 2 h
OPC-AAMK	Ambient water	Immersion in water at 20°C
	Temperature difference cycling	Immersion in water at 20°C for 2 h and at 80°C for 2 h
	Dry-wet cycling	Immersion in water at 20°C for 2 h and drying at 80°C for 2 h

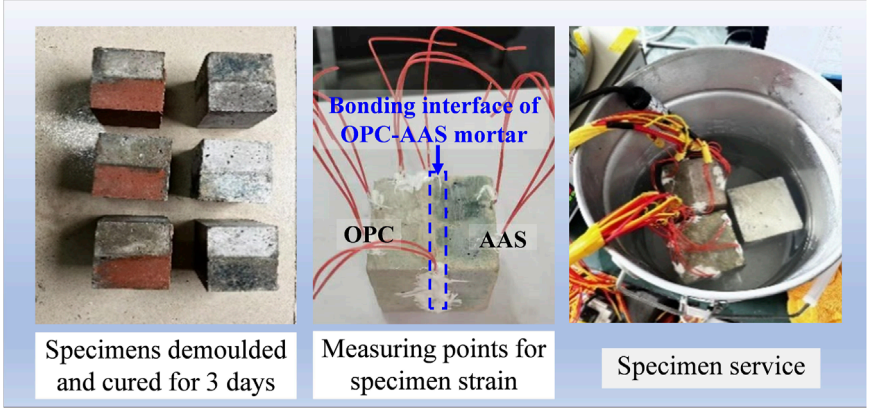

FIGURE 2
Schematic diagram of specimen strain measuring points.

up the test, the wet-dry cycling is varied by heating the oven to 80°C for rapid drying (2 h) and ambient water of 20°C for 2 h to simulate the wetting process.

2.3 Property tests

2.3.1 Expansion shrinkage strain test

The data were extracted by using vibrating string strain gauges with two strain gauges on the OPC side of the composite mortar, at the interfacial bond, and on the alkali-activated geopolymer side. The specific locations of the test points for the specimens are shown in Figure 2: ① Arrange four vibrating string strain gauges along the longitudinal direction at the position of the center of the slab surface on the upper surface of the composite at the alkali-activated geopolymer side and on the lower surface at the OPC side to measure the expansion and shrinkage strains; ② At the position of the center of the bonding interface of the composite, 2 vibrating string strain gauges were arranged along the longitudinal direction to monitor the expansion and shrinkage strain of the bonding interface of the composite mortar. The data for each measurement point was recorded by machine reading and collected once every 20 s. The total test duration was 12 h. The data for each measurement point was recorded by machine reading and collected once every 20 s. The total test duration was 12 h.

2.3.2 Bond strength of the interface

According to ASTM C496 (C Astm, 2011), a split tensile test was used to evaluate the interfacial bond strength of OPC-AAS composite and OPC-AAMK composite mortar. In addition, pure OPC mortars and pure alkali-activated mortars were prepared for further comparison. As shown in Figure 3, two steel bands were placed at the bottom and top of the specimen before the start of the test so that the tensile force was evenly distributed. The sample was loaded at a rate of 0.05 kN/s at the beginning of the test. The load at destruction was measured to obtain Fu, and the splitting strength τu of the specimen was calculated using Equation 1:

$$\tau_u = \frac{2F_u}{\pi bh} \tag{1}$$

where b is the interface length, b = 70.7 mm; h is the height of the cross-sectional dimension of the bonding interface, h = 70.7 mm.

2.3.3 Scanning electron microscope (SEM)

In order to explore the effects of temperature difference cycling, dry-wet cycling on the interfacial bonding strength of OPC-AAS and OPC-AAMK composites, scanning electron microscopy (SEM)

FIGURE 3
Test device of splitting strength.

was used to observe the microstructures of the bonding interfaces of OPC-AAS and OPC-AAMK composites before and after service in different environments. Before observing the micro-morphological characteristics of the interfaces, the specimens were processed by selecting broken specimens containing clear transition interfaces after strength testing and soaking them in acetone solution for 3 days to terminate their hydration. After 3 days, the fragments were removed and dried in a vacuum drying dish, injected with resin, smoothed out in cross-section, and sealed in specimen bags to prevent carbonization. After the specimens were sprayed with gold, the microstructure was observed using a Hitachi S-3400N scanning electron microscope manufactured by Suzhou Sainz Instruments Co.

3 Results and discussion

3.1 Early shrinkage strain of gradient-structured composite

3.1.1 Ambient water

The expansion and shrinkage curves of OPC-AAS and OPC-AAMK composites cured for 3 days in ambient water environment are shown in Figure 4. In general, with the increase of time, OPC, AAS, and AAMK specimens immersed inside the ambient water are always in the state of expansion, and the values of expansion are all increasing. This is mainly because the change of internal humidity is the driving force of specimen shrinkage and deformation (Jun et al., 2010); while the composite has been in ambient water, the drying shrinkage of the specimen is almost nonexistent under the environmental conditions of sufficient humidity, and even the phenomenon of wet swelling leads to the specimen expanding with the increase of the age of immersion (Liu et al., 2022). In addition, specimens with a curing age of only 3 days were still in the continuous hydration phase. Therefore, the specimens in the ambient water environment remained in an expanded state with the increase in immersion time. The final expansion of specimens was as follows: AAS (389.3 μm) > OPC-AAS (283.9 μm) > AAMK (281.6 μm) > OPC-AAMK (158.8 μm) > OPC (28.5 μm).

Further comparison in Figure 4 shows that the expansion and deformation values of both sides of AAS and AAMK are more significant than those of OPC at the same age, while the expansion at the bonding interfacial of OPC-AAS and OPC-AAMK composite is more stable and the deformation curves are smoother than those of the corresponding AAS and AAMK sides. Figure 4A indicates that the expansion strain of the AAS is always the largest, and the final expansion strain of bonding interface of the OPC-AAS composite is 27.07% lower than the final expansion of AAS. This is because the bonding interface of the OPC-AAS composite may has produced new hydration products during the hydration reaction, and the lower heat of hydration produced by this hydration reaction will result in a lower temperature rise within the concrete, which will lead to a decrease in the expansion of concrete (Wang et al., 2012). Figure 4B shows that the development trend of the shrinkage strain curve of the OPC-AAMK composite is basically the same as that of the OPC-AAS composite. However, the magnitude of the strain is different, and the final expansion of the bonding interface of the OPC-AAMK composite is only 158.8 μm, which is 43.61% lower than that of the AAMK side.

3.1.2 Temperature difference cycling

The early shrinkage curves of OPC-AAS and OPC-AAMK composites under temperature difference cycling conditions are shown in Figure 5. In order to analyze better the effect of temperature difference cycling on the shrinkage and deformation of the gradient-structured composites, the shrinkage at the warming-cooling node of the three cycles is plotted as shown in Figure 6.

Figure 5 shows that the gradient-structured composites undergo the first temperature increase from 0 h to 2 h. Compared with the OPC side of the specimen that expands with temperature increase, the bonding interface and the alkali-activated material (AAM) portion of the laminated specimen shrinks with temperature increase. This may be due to the fact that the laminated specimen is a combination of AAM and OPC, and the first temperature increase caused the OPC side to expand continuously, while the expansion values of the bonding interface and the pure AAM side were smaller than those of the OPC under the temperature change, thus, under the expansion of the OPC, it resulted in the extrusion at the interface between the AAM and the bonding, and the greater the contraction with the increase of the environmental temperature. When the environmental temperature was first stabilized at 80°C, the internal structural deformation of the specimen had been completed, allowing the composite structure to re-achieve a stable state. The shrinkage-deformation curves for 2 ~ 12 h after the gradient-structured composites were stabilized illustrate that warming leads to expansion of the specimen and cooling leads to shrinkage of composites. Compared with the shrinkage-deformation curves of pure cement and alkali-activated materials, the shrinkage-deformation curves at the bonding interfacial of gradient-structured composites under temperature difference cycling were smoother, and the fluctuation amplitude of shrinkage-deformation during the whole process of warming-up-lowering-down was lower. This may be due to the overall properties of the specimen, which causes the AAM side to be squeezed and in contraction when the overall expansion value on the OPC side is more significant, a phenomenon that occurs at both the OPC-AAMK and OPC-AAS bonding interfaces. Figure 6 shows that with the increase in cycles, the strain difference between the specimens at the rising and falling temperature points decreases accordingly. The AAS and AAMK specimens were in a shrinkage state, with final shrinkage strains

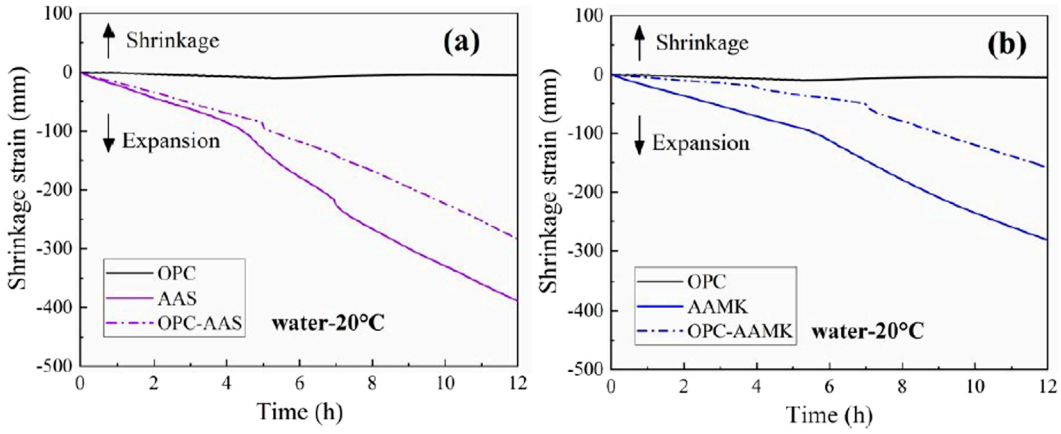

FIGURE 4
Shrinkage strain of OPC-AAS composites **(A)** and OPC-AAMK composites **(B)** in room temperature water.

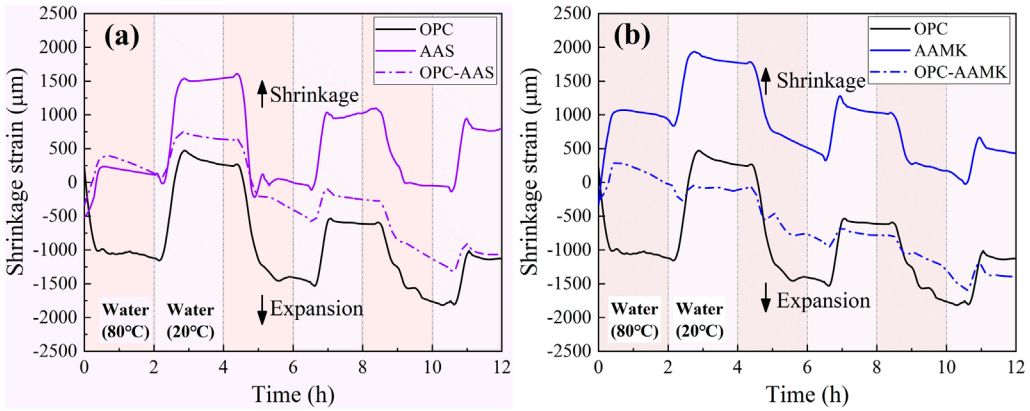

FIGURE 5
Shrinkage strain of OPC-AAS composites **(A)** and OPC-AAMK composites **(B)** under temperature cycling conditions.

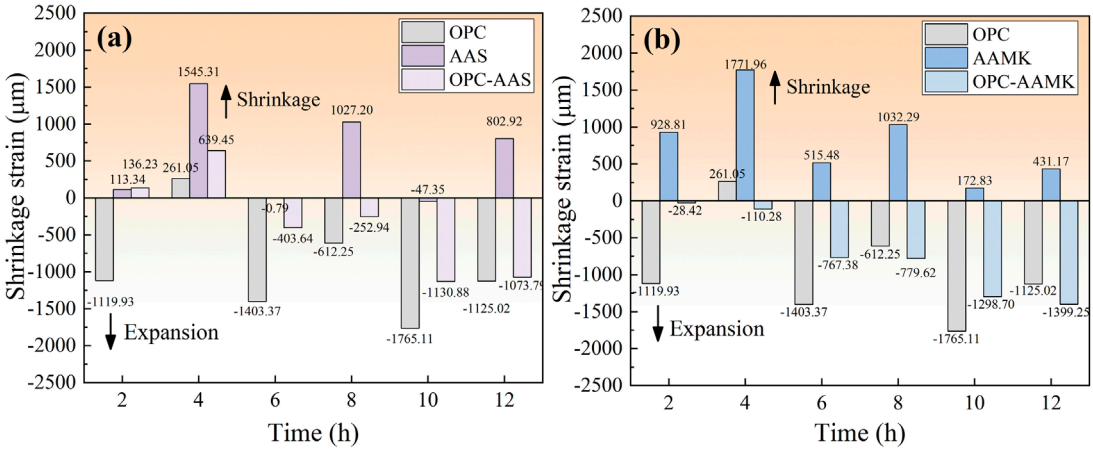

FIGURE 6
Expansion and shrinkage values of OPC-AAS composites **(A)** and OPC-AAMK composites **(B)** at the rising-falling temperature node.

of 802.92 μm and 431.17 μm, respectively, whereas the bonding interfaces of OPC, OPC-AAS and OPC-AAMK composites were in an expansion state, with the final expansions of OPC-AAMK (1,399.25 μm) > OPC (1,125.02 μm) > OPC- AAS (1,073.79 μm).

3.1.3 Dry-wet cycling

The shrinkage and deformation curves of OPC-AAS and OPC-AAMK composites under dry-wet cycling are shown in Figure 7. The shrinkage of the specimens at the nodes of the rising drying and ambient water are demonstrated in Figure 8. Overall, the effect of environmental humidity changes on the shrinkage strain at the OPC as well as at the bonding interface of OPC-AAMK composite was not significant. The expansion and contraction stage of the OPC was the most stable. Still, the dry-wet cycling significantly affected the shrinkage strain of the bonding interface of OPC-AAS composite and the AAS specimen during the hydration process. The shrinkage-deformation results in Figure 7 indicate that the specimens were first dried and raised to 80°C from 0 h to 2 h. The deformation curves of the OPC specimens and the OPC-AAMK composite contracted with the increase in drying time, whereas the deformation curves of both the AAS specimens and the OPC-AAS composite swelled with the increase in drying time, which is different from that of the results in Figure 5A for the water-bath rising to 80°C. Further observation of the shrinkage-deformation curves from 2 to 12 h shows that the shrinkage-deformation curves of composite under the cycle of drying and rising temperature and immersion in ambient water show a trend of linear rise and then slow rise and finally contraction. I (linear rise): the specimen from 20°C water-saturated environment to 80°C dry environment, the specimen due to rising temperature and make the specimen as a whole orderly expansion; II (slowly rising): when the temperature reaches a certain value, the specimen began to appear drying under the loss of water contraction, which led to a slow rise in the specimen expansion; III (shrinkage decline): the specimen stabilized in the dry environment of 80°C, the specimen at this time the internal temperature and the environmental temperature is consistent with the temperature of the specimen, temperature on the expansion of the expansion of the value of the influence of small, but the internal water due to the drying of the continuing However, the internal moisture loss due to drying continues, resulting in the gradual shrinkage of the specimen.

Figure 8 shows that with the increase in the number of dry-wet cycling, the strain difference between the specimens at the dry-wet node is decreasing accordingly. The strain fluctuation at the bonding interface of OPC-AAS composite is the most drastic, with the highest expansion and shrinkage values of 785.45 μm and 360.30 μm, respectively; whereas the fluctuation of the strain curve at the bonding interface of OPC-AAMK composite under the conditions of dry-wet cycling is very small, with the highest expansion and shrinkage values of 150.3 μm and 77.65 μm, respectively. This further indicates that the effect of dry-wet cycling on the shrinkage and deformation at the interface of OPC-AAS composite is more obvious.

3.1.4 Comparative analysis of extreme environments

Figures 9A, B represent the shrinkage strains of the gradient-structured composites in extreme environments, and Figures 9C, D show the difference between the shrinkage strains of the two extreme environments for the shrinkage strains at ambient water. Figures 9A, B shows that the strain of the composites in extreme environments increases significantly compared to the strain values of the ambient water. For the same number of cycles, the strain values of OPC-AAS and OPC-AAMK composites under temperature difference cycling are larger than that of dry-wet cycling, and the expansion values with the largest change in amplitude in the shrinkage strain test under temperature difference cycling are 1,130.88 μm and 1765 μm, respectively, which are much higher than that of the maximum expansion values of 785.45 μm and 150.30 μm for the dry-wet cycling. In addition, Figures 9C, D show that after three cycles, the strain difference between the OPC-AAS and OPC-AAMK composites under the effect of temperature difference cycling and ambient water is 789.89 μm and 1,240.45 μm, respectively, while the strain difference between dry-wet cycling and ambient water is 374.75 μm and 8.5 μm, respectively, which further suggests that the effect on the interfacial shrinkage strain due to temperature difference cycling is much larger than that due to dry-wet cycling.

3.2 Early interfacial bonding strength of gradient-structured composite

3.2.1 Temperature difference cycling

Figure 10 shows the splitting strength of gradient-structured composites under different temperature cycling, and the corresponding splitting strength values are shown in Table 4. It can be seen that the splitting strengths of OPC and AAS specimens showed a gradual increase with cycling, and were 1.54 MPa and 3.84 MPa after three cycles, which were 130.77% and 29% higher than the initial values, respectively. In contrast, the splitting strength of AAMK specimen showed a decreasing trend, with a 51.94% decrease from the initial value after three cycles. It is possible that the unhydrated cement particles and AAS system continue to hydrate, which improves the densification and strengthens the concrete, while the AAMK system slows down the reaction and reduces the amount of water bound to the products, which increases the proportion of free water in the system and accelerates the rate of water loss, so that there is a continuous decrease in the splitting strength (Kuenzel et al., 2012). In addition, the bonding strength of OPC-AAS composite increased more than that of OPC-AAMK composite in the early stage of cycling under temperature cycling conditions, while the damage was more negligible in the later stage of cycling. With the number of cycles increases, both OPC-AAS and OPC-AAMK composites showed the change rule of increasing first (strengthening stage) and then decreasing (deterioration stage). They reached the maximum value at two times cycles, which was 2.66 MPa and 2.53 MPa, respectively, and increased by 23.75% and 10.43% compared with the initial value.

3.2.2 Dry-wet cycling

Figure 11 shows the splitting strength of mortar under different times of dry-wet cycling, and the specific splitting strength values are shown in Table 4. It can be seen that the change rule of splitting strength under the action of the

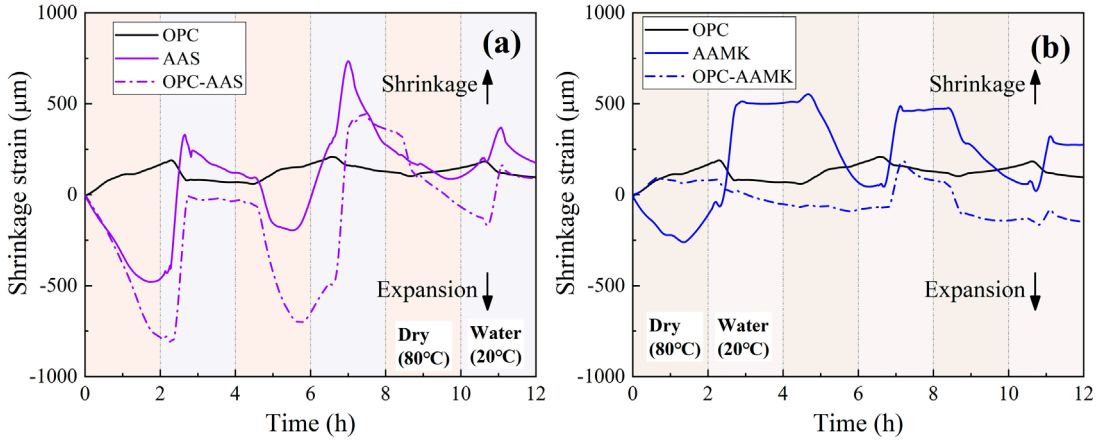

FIGURE 7
Shrinkage strain of OPC-AAS composites **(A)** and OPC-AAMK composites **(B)** under wet-dry cycling conditions.

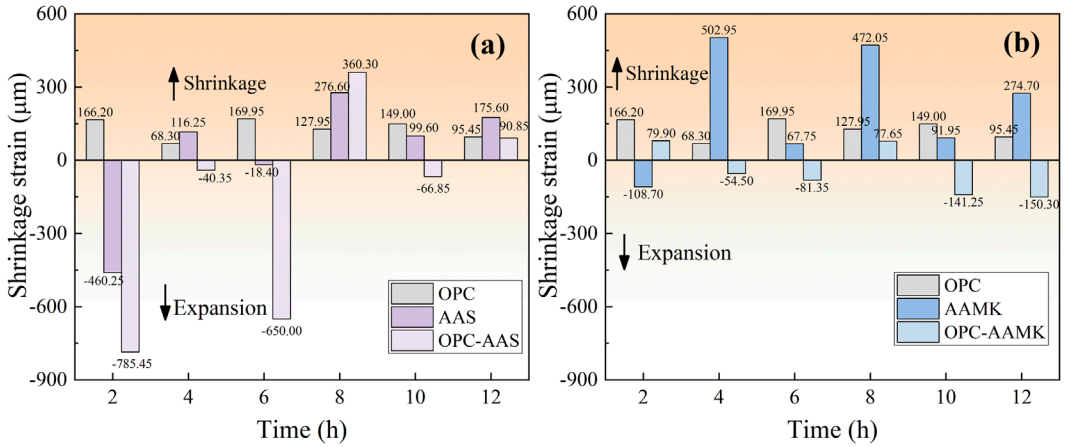

FIGURE 8
Shrinkage strain values of OPC-AAS composites **(A)** and OPC-AAMK composites **(B)** at high temperature drying-normal temperature immersion node.

dry-wet cycling is consistent with the change rule under the temperature difference cycling, but the splitting strength of specimens under the dry-wet cycle seems to grow higher. After three dry-wet cycles, the splitting strength of OPC and AAS specimens increased by 253.85% and 74.46% compared to the initial values, while AAMk specimen lost only 6.77% of its splitting strength compared to the initial value. Similarly, the OPC-AAS and OPC-AAMK composites showed the change rule of increasing first (enhancement stage) and then decreasing (deterioration stage), both of which reached the maximum value at two times wet-dry cycles, 3.65 MPa and 2.69 MPa, respectively, which increased 69.81% and 17.41%, respectively, compared with the initial value. In addition, according to the results in Figures 10, 11, we can correlate the splitting strength under extreme environmental service with the number of cycles to establish a correlation model, and according to Figure 12, the splitting strength and the number of cycles present a quadratic correlation and have a high correlation.

3.2.3 Comparative analysis of extreme environments

Figure 13 compares the splitting strength of the composite after three cycles in both environments, and Figure 14 shows the image of the composite bonding interface before and after splitting. In general, the splitting strengths of composites after three cycles in the same environment are OPC-AAS > OPC-AAMK. In addition, comparing the rate of loss of splitting strength before and after service in the two environments, it can be seen that the deterioration of the interface caused by the temperature difference cycling is more significant than that of the interface caused by the dry-wet cycling. From Figure 14, it can be seen that there is a clear difference between the specimens with temperature difference cycling and those with

10.3389/fmats.2025.1527502

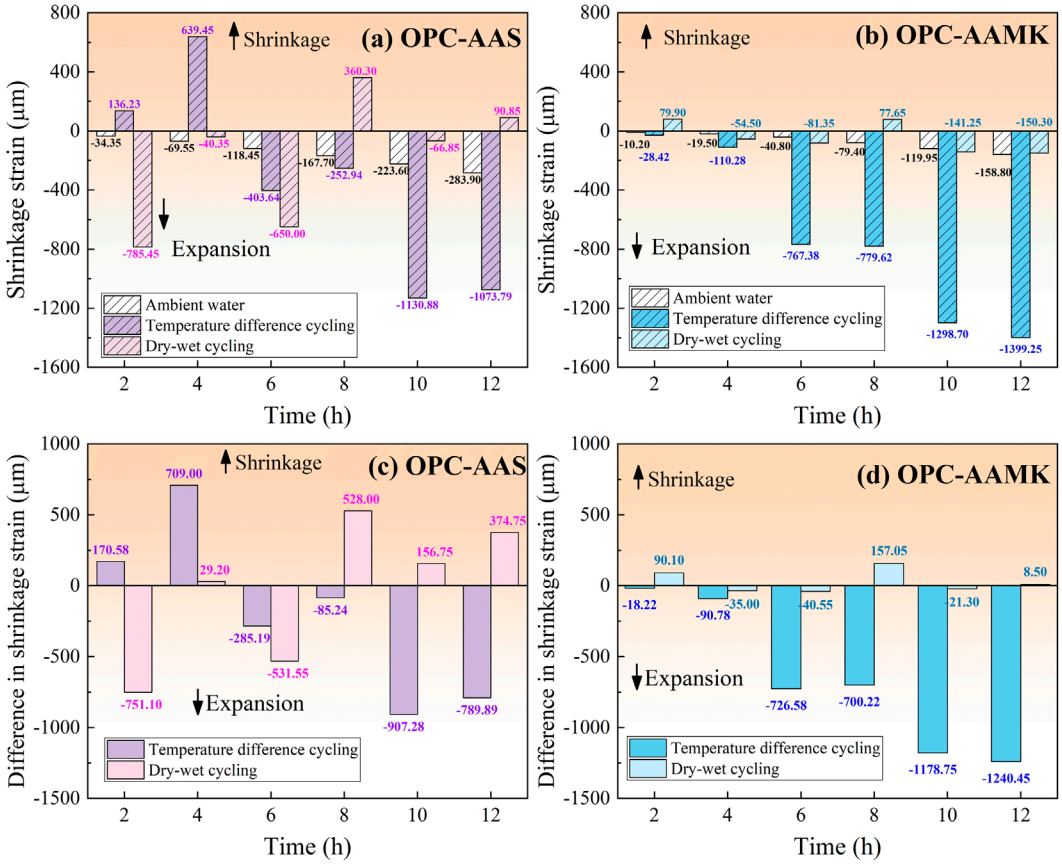

FIGURE 9
Shrinkage strains in different environments **(A)** OPC-AAS, **(B)** OPC-AAMK and the difference of shrinkage strains **(C)** OPC-AAS, **(D)** OPC-AAMK.

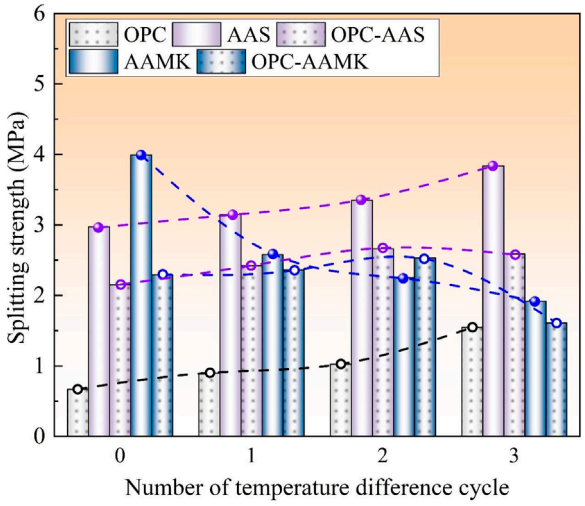

FIGURE 10
Splitting strength of composites under temperature difference cycling.

wet-dry cycling. The specimens with temperature difference cycling can be observed to have more severe interfacial degradation after splitting, with irregular powder layer shedding in some areas. In contrast, the specimens with wet-dry cycling have more uniform and regular delamination in the interfacial area after splitting. This may be because humidity affects the development of pore structures in geopolymer systems. Low humidity increases surface tension and capillary pressure, which destroys the initially dense reticulated gel phase, reducing the strength of alkali-activated cementitious materials (Huang et al., 2024). The large temperature difference not only affects the release rate of water molecules, resulting in the slow formation of the gel phase, so that the strength of AAS and AAMK are reduced (Bonneau et al., 1997), which in turn affects the interfacial bonding strength; it also leads to gradual decomposition of alkali-activated cementitious material products with the rise in temperature, resulting in the microstructural cracking and even the emergence of pores, which further affects the shrinkage and expansion of bonding interfacial properties. Further combined with Figures 5, 7, it can be seen that the specimens have greater expansion and shrinkage values under temperature difference cycling compared to dry-wet cycling, and under such temperature difference cycling conditions, the interfacial shear stresses generated by inhomogeneous expansion between the material components become higher, and with the increase of the number of cycling times, the cleavage values at the composite bonding interfaces decrease. Therefore, the temperature difference cycling has a greater influence

TABLE 4 The splitting strength of composite cycled 3 times in different service environments.

Service environments	Cycle times	Splitting strength (MPa)				
		OPC	AAS	AAMK	OPC-AAS	OPC-AAMK
Temperature difference cycling	0	0.67	2.97	3.99	2.15	2.29
	1	0.90	3.15	2.58	2.20	2.39
	2	1.03	3.35	2.25	2.45	2.65
	3	1.54	3.84	1.92	2.59	1.61
Dry-wet cycling	0	0.67	2.97	3.99	2.15	2.29
	1	1.25	3.35	4.05	2.78	2.45
	2	1.87	4.35	4.12	3.05	2.69
	3	2.37	5.19	3.72	3.51	2.34

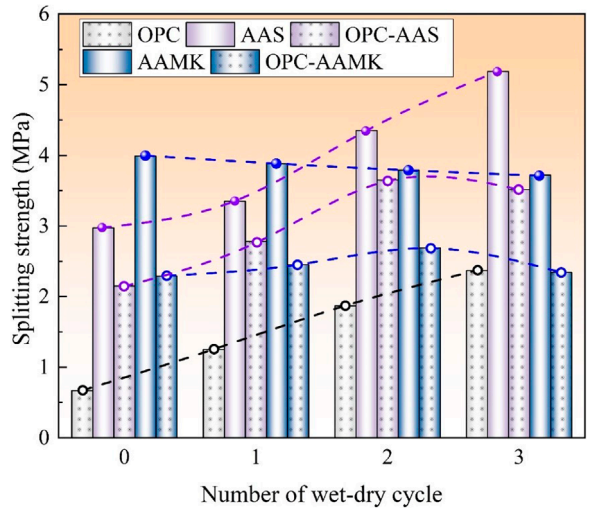

FIGURE 11
Splitting strength of composite under wet and dry cycling conditions.

on the splitting strength at the interface of gradient-structural composites.

3.3 Microstructural analysis of bonding interfaces

Figure 15 shows the SEM images of OPC-AAS and OPC-AAMK composites before and after service in different environments. Figures 15A, D can be observed that the transition line at the bonding interfacing of OPC-AAS and OPC-AAMK composites are more evident at ambient water, and the material and structure distribution at the interface of the composite is different on both sides. The OPC region of the OPC-AAMK composite is primarily dark grey colloidal material with brighter aggregates. In contrast, the AAMK region is dominated by grey, with an incompletely hydrated high territory (Nie et al., 2019). Clear interfacial lines were also observed in the OPC-AAS composite, with most of the AAS region cementitious and the specimen surfaces denser. Figures 15B, E show that after temperature cycling of OPC-AAMK composite, there is an obvious interface transition line, and the number of microcracks at the bond interface is obviously increased. The cracks are enlarged, including long straight cracks penetrating through the bonding interface of the material, cracks spreading to the surrounding area, shorter tortoise-like cracks, and large holes. Additionally, although many microcracks exist on both sides of the interface of OPC-AAS composite, the bonding interface is better. In contrast, Figures 15C, F show that the transition line at the bonding interfacial of composite is pronounced after wet-dry cycling. However, the interface are no cracks and holes around the OPC-AAS, and the whole is still relatively dense, whereas cracks appear on the OPC side of the OPC-AAMK composite, and there are apparent large holes on the AAMK side.

The forming of hole and cracks also corresponds to the interfacial splitting strength in Table 4. The hydration degree of OPC and AAS speciemen is lower. The enhancement effect brought by hydration is greater than the damage caused by temperature difference cycling and dry-wet cycling, which also leads to a continuous increase in splitting strength. In contrast, the rehydration of composite is weakened for OPC-AAS and OPC-AAMK composites (Zhouping and Yang, 2021), with the continuation of temperature difference cycling or dry-wet cycling. With the continuation of the temperature difference cycling or dry-wet cycling process, the rehydration of composite is weakened. The continuous cycle leads to the accumulation of internal damage in concrete and even induces some new cracks and defects, in which the microstructure degradation of OPC-AAMK is more serious; the strength of concrete and its microstructure has a very close connection, and the change of internal microstructure of composite explains the change rule of the composite splitting strength which firstly increases and then decreases.

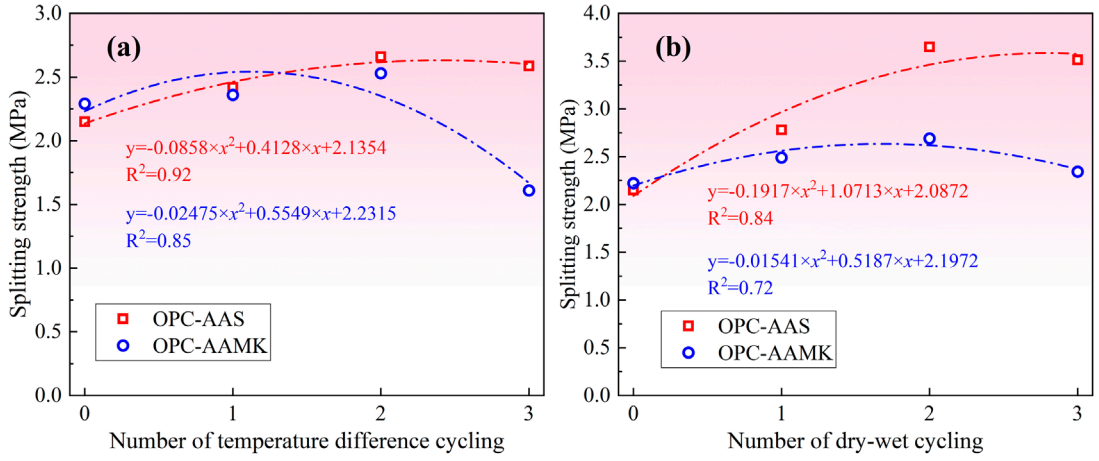

FIGURE 12
Relationship between the splitting strength and the number of cycles of OPC-AAS composites **(A)** and OPC-AAMK composites **(B)** under extreme environmental service.

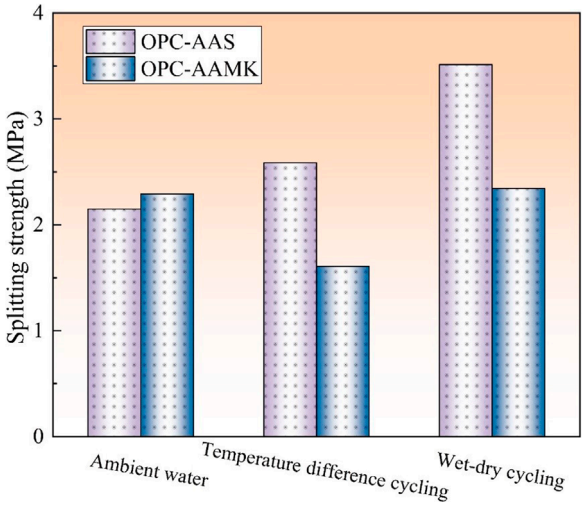

FIGURE 13
Splitting strength of gradient-structural composites after three times cycling in different service environments.

4 Discussion

The purpose of this section is to further discuss the changes in shrinkage deformation and interfaces bonding strength at the OPC-AAS and OPC-AAMK composites in service under both temperature difference cycling and dry-wet cycling conditions. Based on the results of the above characterization tests, comparing the ambient water environments, it was found that different extreme environments (e.g., under thermal cycling from high temperature to low temperature, and under humidity cycling from immersion to drying) had a significant effect on the shrinkage deformation, strength evolution, and microstructures of the gradient-structured composites. Based on the results of this study, the performance evolution mechanism of the bonding interface of gradient-structured composites under different service conditions is analyzed as follows.

4.1 Gradient-structured composites under temperature difference cycling

The interfacial resistance to shrinkage of the OPC-AAS and OPC-AAMK composites under temperature difference cycling has been increasing, and OPC-AAMK has a stronger resistance to shrinkage under the effect of temperature difference cycling (Figures 5–8). This is due to the fact that the combination of different AAMK and AAS with OPC to form the gradient-structured composites can reduce the shrinkage properties of the alkali-activated material, respectively, and in addition, the high temperature condition facilitates the further hydration of the interface of the gradient-structured composites, which can reduce the shrinkage strain of the composites and improve the bonding properties of the interface. As the number of temperature difference cycling increases, the unhydrated cement particles and AAS materials continue to hydrate at shorter curing ages, which improves the densification and strengthens the composites, causing a higher enhancement than deterioration of the interfacial bonding properties of OPC-AAS, resulting in the overall cleavage strength still being enhanced (Figure 10); whereas the AAMK system slows down the reaction rate and reduces the amount of water bound to the products, thus increasing the proportion of free water in the system and accelerating the rate of water loss, resulting in a continuous decrease in the splitting strength (Figure 11). From the SEM results, it was further demonstrated that under the temperature difference cycling conditions, OPC-AAMK not only showed cracks at the interface, but also observed the generation of more holes around it (Figures 15C, F).

In conclusion, a large temperature difference not only affects the release rate of water molecules, resulting in slow gel phase formation, which reduces the strength of AAS and AAMK,

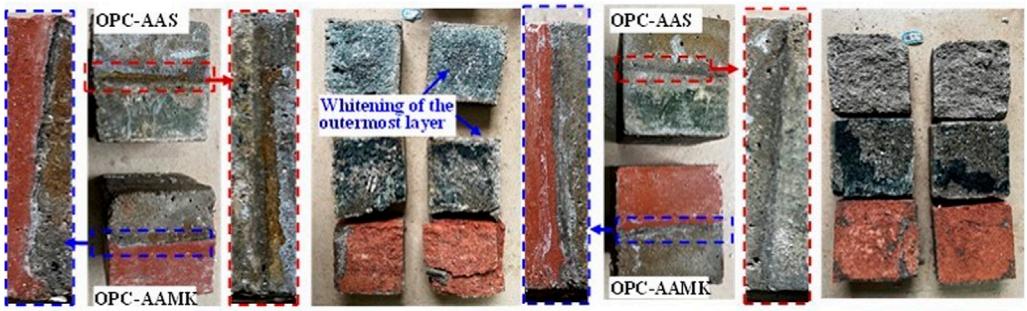

FIGURE 14
Pictures of gradient-structural composites after three times cycling in different service environments. **(A)** Temperature difference cycling **(B)** Dry-wet cycling.

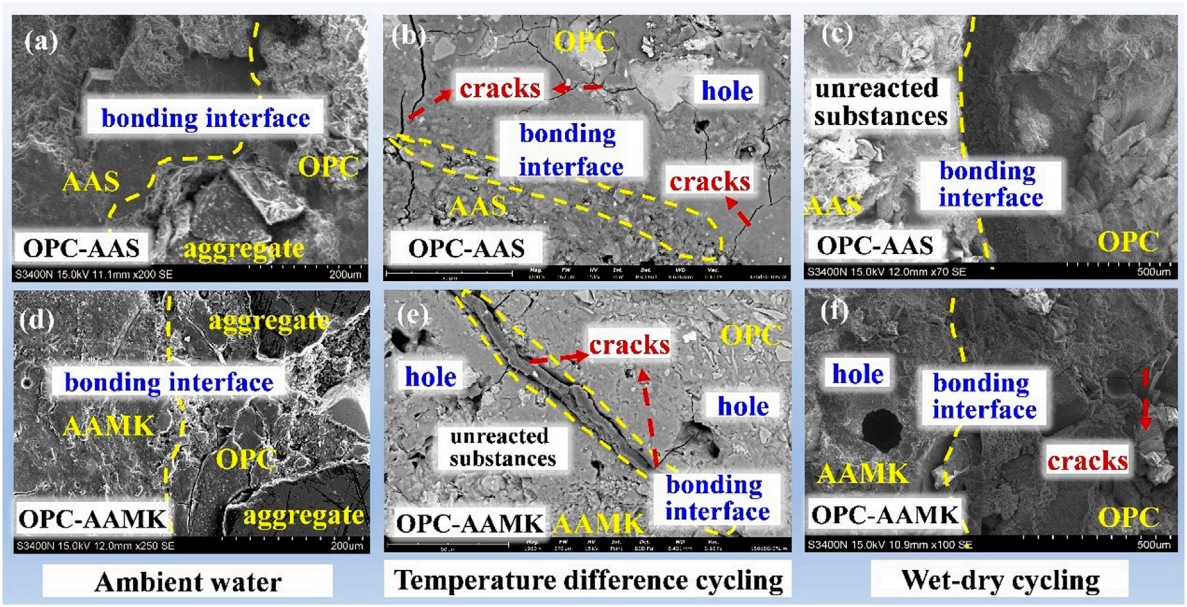

FIGURE 15
SEM images of bonding interfaces of composites in different service environments: **(A–C)** OPC-AAS composites in Ambient water, Temperature difference cycling and Wet-dry cycling; **(D–F)** OPC-AAMK composites in Ambient water, Temperature difference cycling and Wet-dry cycling.

and thus affects the bond strength of the interface; it also leads to the gradual decomposition of alkali-activated material products with increasing temperature, resulting in microstructural cracking, and even the appearance of pores (Figure 15), which further affects the shrinkage and expansion of bonded interfacial properties (Bonneau et al., 1997).

4.2 Gradient-structured composites under dry-wet cycling

The pattern of change in the interfacial splitting strength of composite is also a result of the combined effect of the enhancement effect caused by the hydration reaction of the unhydrated cement particles and the deterioration effect produced by the damage accumulated in the dry and wet cycles. On the one hand, unhydrated cementitious materials continue to hydrate (e.g., cement particles, slag, biotite territories), thus improving the densification of the concrete and enhancing the concrete interfacial bond strength. However, humidity affects the rate of water molecule release and pore structure development in the alkali excitation system (Figure 15). Due to the difference in water vapor pressure, the gas escapes outwards in the drying process, further enlarging the concrete's internal pores or leading to new pores and defects. In the wetting process, due to the existence of capillary force, the environment of water is drawn into the internal pores of concrete, resulting in pore expansion, so the continuous wet and dry cycle will inevitably lead to a further increase in the damage, the strength of concrete has a weakening effect (Figure 10) (Yaman et al., 2002).

5 Conclusion

In this paper, the temperature difference cycling, dry-wet cycling conditions were all affect the OPC-AAS and OPC-AAMK composites of for both macro contraction and microstructure, especially on the early stage of bonding interface. The main conclusions are as follows:

(1) The effect of temperature difference cycling on the shrinkage strain at the bonding interface of composites is greater than that of wet-dry cycling. After three cycles, the strain difference between OPC-AAS and OPC-AAMK composites was 789.89 μm and 1,240.45 μm under temperature difference cycling and ambient water, respectively, while the strain difference between dry-wet cycling and ambient water was 374.75 μm and 8.5 μm, respectively.

(2) The early splitting strength of OPC-AAS composites in extreme environments was greater than that of OPC-AAMK composites. Comparing with dry-wet cycling, the splitting strength of OPC-AAS and OPC-AAMK composites decreased even more severely after 3 cycles of temperature difference, by 26.37% and 31.32%, respectively.

(3) The SEM results show that the degradation of the interface microstructure caused by temperature differential cycling is also greater than that caused by wet and dry cycling. The differential temperature cycling leads to the gradual decomposition of the products of AAMK cementitious materials with temperature rise, resulting in the deterioration of the microstructure of the OPC-AAMK interface and even the emergence of cracks and holes in the bond interface, and the deterioration of the splitting strength.

Prospects and suggestions: The focus of this present study is on the influence of temperature difference cycling and dry-wet cycling effects on the interfacial bonding properties of gradient-structural composites, which are important for the application of gradient-structural composites in extreme environments with temperature and humidity variations. However, the current manuscript has some limitations and does not discuss cost-effectiveness. In addition, scientific attention and efforts should also be directed toward other aggressive and complex environments, such as sole chemical exposures to chloride ions, sulphate ions, or compound exposures to chloride-sulphate attack, as well as other potential physicochemical aggressions such as freeze-thaw cycling and salt-freeze cycling.

Data availability statement

The original contributions presented in the study are included in the article/supplementary material, further inquiries can be directed to the corresponding author.

Author contributions

XL: Data curation, Investigation, Writing–original draft. GJ: Data curation, Investigation, Writing–original draft. NW: Data curation, Writing–original draft. YW: Data curation, Formal Analysis, Investigation, Writing–original draft. ZC: Funding acquisition, Validation, Writing–review and editing. JL: Validation, Writing–review and editing. BC: Methodology, Writing–original draft. JY: Investigation, Validation, Writing–original draft.

Funding

The author(s) declare that financial support was received for the research, authorship, and/or publication of this article. The authors sincerely acknowledge the financial support by Guangxi Science and Technology Major Program of China (GKAA23073017, GKAA23023034, GKAA23062034).

Conflict of interest

Authors SL, NW, and YW were employed by Guangxi Road and Bridge Engineering Group Co. Author GJ was employed by Guangxi Guanglu Industrial Investment Group Co.

The remaining authors declare that the research was conducted in the absence of any commercial or financial relationships that could be construed as a potential conflict of interest.

Generative AI statement

The author(s) declare that no Generative AI was used in the creation of this manuscript.

Publisher's note

All claims expressed in this article are solely those of the authors and do not necessarily represent those of their affiliated organizations, or those of the publisher, the editors and the reviewers. Any product that may be evaluated in this article, or claim that may be made by its manufacturer, is not guaranteed or endorsed by the publisher.

References

Benito, P., Leonelli, C., Medri, V., and Vaccari, A. (2013). Geopolymers: a new and smart way for a sustainable development. *Appl. Clay Sci.* 73, 1. doi:10.1016/j.clay.2013.03.008

Bonneau, O., Mohamed, L., Dallaire, E., Dugat, J., and Aitcin, P.-C. (1997). Mechanical properties and durability of two industrial reactive powder concretes. *Mater. J.* 94 (4), 286–290. doi:10.14359/310

C Astm (2011). *Standard test method for splitting tensile strength of cylindrical concrete specimens*. West Conshohocken, PA: C ASTM Intemational, 496.

Chen, Z., Chen, B., Tang, Y., Zhao, G., Pang, Z., and Shi, C. (2024b). Innovative strategies for time-release PCE design and cement paste flowability control. *Cem. Concr. Compos.* 154, 105785. doi:10.1016/j.cemconcomp.2024.105785

Chen, Z., Huang, Z., Wei, J., Zhao, G., and Tang, Y. (2024c). The mechanical properties and chlorine resistance of concrete based on the effects of pouring interval time. *Buildings* 14 (6), 1558. doi:10.3390/buildings14061558

Chen, Z., Peng, Y., and Li, C. (2021). Experimental study for the adhesive interface mechanical properties of double lapped steel-CFRP plate at high temperature. *Acta Mater Compos. Sin.* 38 (02), 449–460. doi:10.13801/j.cnki.fhclxb.20200608.002

Chen, Z., Wu, C., Luo, X., Wen, Xu, Liang, W., and Tang, Y. (2024a). Spatio-temporal autogenous shrinkage and cracking behavior of core concrete in full-scale CFST: insights from the world's largest span arch bridge. *Thin-Walled Struct.* 200, 111899. doi:10.1016/j.tws.2024.111899

Chen, Z., Yu, J., Nong, Y., Yang, Y., Zhang, H., and Tang, Y. (2023). Beyond time: enhancing corrosion resistance of geopolymer concrete and BFRP bars in seawater. *Compos. Struct.* 322, 117439. doi:10.1016/j.compstruct.2023.117439

Chen, Z., Zhao, G., Wei, J., Chen, C., and Tang, Y. (2024d). Residual impact resistance behavior of PVA fiber reinforced cement mortar containing Nano-SiO2 after exposure to chloride erosion. *Constr. Build. Mater.* 414, 134990. doi:10.1016/j.conbuildmat.2024.134990

Dai, T., Fang, C., Liu, T., Zheng, S., Lei, G., and Jiang, G. (2024). Waste glass powder as a high temperature stabilizer in blended oil well cement pastes: hydration, microstructure and mechanical properties. *Constr. Build. Mater.* 439, 137359. doi:10.1016/j.conbuildmat.2024.137359

Davidovits, J. (2018). Geopolymers based on natural and synthetic metakaolin a critical review; proceedings of the proceedings of the 41st international conference on advanced ceramics and composites: ceramic engineering and science proceedings. *Wiley Online Libr.* 38 (3). doi:10.1002/9781119474746.ch19

Dybeł, P., and Kucharska, M. (2020). Effect of bottom-up placing on bond properties of high-performance self-compacting concrete. *Constr. Build. Mater.* 243, 118182. doi:10.1016/j.conbuildmat.2020.118182

Fang, Y., Pan, J., and Christopher, K. Y. L. (2013). Flexural behaviors of ECC and concrete/ECC composite beams reinforced with basalt fiber-reinforced polymer. *J. Compos. Constr.* 17 (5), 591–602. doi:10.1061/(asce)cc.1943-5614.0000381

Gao, S., Chen, Y., Lin, P., Liang, Xu, Wang, J., and Lu, L. (2020). Effect of high temperature on the mechanical properties of alkali-stimulated ultra-high performance concrete. *Bull. Chin. Ceram. Soc.* 39 (09), 2815–2820. doi:10.16552/j.cnki.issn1001-1625.20200602.003

He, L., Chen, B., Liu, Q., Chen, H., Hua, Li, Chow, W. T., et al. (2024a). A quasi-exponential distribution of interfacial voids and its effect on the interlayer strength of 3D printed concrete. *Addit. Manuf.* 89, 104296. doi:10.1016/j.addma.2024.104296

He, L., Pan, J., Hee, Yu S., Chen, H., Gu Li, L., Panda, B., et al. (2024b). Development of novel concave and convex trowels for higher interlayer strength of 3D printed cement paste. *Case Stud. Constr. Mater.* 21, e03745. doi:10.1016/j.cscm.2024.e03745

Hu, K., Chen, Z., Kang, H., and Tang, Y. (2024). 3D vision technologies for a self-developed structural external crack damage recognition robot. *Automation Constr.* 159, 105262. doi:10.1016/j.autcon.2023.105262

Huang, D., Wang, Z., Tang, W., Zhang, Q., and Xiaohu, Q. (2024). Influence of conservation environment on the properties and microstructure of metakaolin base aggregates. *Bull. Chin. Ceram. Soc.* 43 (04), 1463–1471. doi:10.16552/j.cnki.issn1001-1625.20240131.003

Ikumi, T., Cavalaro, S. H. P., Segura, I., Albert De La Fuente, and Aguado, A. (2016). Simplified methodology to evaluate the external sulfate attack in concrete structures. *Mater. and Des.* 89, 1147–1160. doi:10.1016/j.matdes.2015.10.084

Jamal Jumaah, H., Rashid, A. A., Saleh, S. A. R., and Jamal Jumaah, S. (2024). " Deep Neural Remote Sensing and Sentinel-2 Satellite Image Processing of Kirkuk City, Iraq for Sustainable Prospective. Journal of Optics and Photonics Research.

Jiu-Jun, Y., Ran, H., Yan-Ling, D., and Ke-Ru, Wu. (2003). Effects of the component and fiber gradient distributions on the strength of cement-based composite materials. *J. Wuhan Univ. Technology-Mater Sci Ed* 18 (2), 61–64. doi:10.1007/bf02838805

Jun, T., Wu, X., Zheng, Yu, Hu, S., Du, Y., Wang, W., et al. (2019). Investigation of interface shear properties and mechanical model between ECC and concrete. *Constr. Build. Mater.* 223, 12–27. doi:10.1016/j.conbuildmat.2019.06.188

Jun, Z., Hou, D., and Sun, W. (2010). Experimental study on the relationship between shrinkage and interior humidity of concrete at early age. *Mag. Concr. Res.* 62 (3), 191–199. doi:10.1680/macr.2010.62.3.191

Keita, E., Bessaies-Bey, H., Zuo, W., Belin, P., and Roussel, N. (2019). Weak bond strength between successive layers in extrusion-based additive manufacturing: measurement and physical origin. *Cem. Concr. Res.* 123, 105787. doi:10.1016/j.cemconres.2019.105787

Kuenzel, C., Vandeperre, L. J., Donatello, S., Boccaccini, A. R., and Cheeseman, C. (2012). Ambient temperature drying shrinkage and cracking in metakaolin-based geopolymers. *J. Am. Ceram. Soc.* 95 (10), 3270–3277. doi:10.1111/j.1551-2916.2012.05380.x

Latif Baloch, W., Siad, H., Mohamed, L., and Sahmaran, M. (2021). A review on the durability of concrete-to-concrete bond in recent rehabilitated structures. *J. Build. Eng.* 44, 103315. doi:10.1016/j.jobe.2021.103315

Li, X., Hu, Y., Jie, Y., Zhao, C., and Zhang, Z. (2024). Dual-frequency lidar for compressed sensing 3D imaging based on all-phase fast fourier transform. *J. Opt. Photonics Res.* 1 (2), 74–81. doi:10.47852/bonviewjopr32021565

Liu, Y., Liao, Y., and Yagang, Li. (2022). Effects of ultrafine slag powder and metakaolin on the early shrinkage properties of sulfoaluminate cement. *Bull. Chin. Ceram. Soc.* 41 (6). doi:10.16552/j.cnki.issn1001-1625.2022.06.024

Liu, Y., Wang, B., Fan, Y., Yu, J., Shi, T., Zhou, Y., et al. (2024b). Effects of reactive MgO on durability and microstructure of cement-based materials: considering carbonation and pH value. *Constr. Build. Mater.* 426, 136216. doi:10.1016/j.conbuildmat.2024.136216

Liu, Y., Wang, B., Qian, Z., Yu, J., Shi, T., Fan, Y., et al. (2024a). State-of-the art on preparation, performance, and ecological applications of planting concrete. *Case Stud. Constr. Mater.* 20, e03131. doi:10.1016/j.cscm.2024.e03131

Ma, B., Gao, Y., Wang, X., and Yu, J. (2006). "Design and material properties of functional gradient concrete pipe sheet," in *The third national commercial concrete information technology exchange conference and the 2006 national commercial concrete annual meeting*. Hangzhou, Zhejiang, China: F.

Matalkah, F., Salem, T., Shaafaey, M., and Soroushian, P. (2019). Drying shrinkage of alkali activated binders cured at room temperature. *Constr. Build. Mater.* 201, 563–570. doi:10.1016/j.conbuildmat.2018.12.223

Meng, Z., Zhang, Y., Chen, W.-kang, Fu, C.-qing, Xiang Xiong, Q., Zhang, C.-lin, et al. (2024). A numerical study of moisture and ionic transport in unsaturated concrete by considering multi-ions coupling effect. *Transp. Porous Media* 151 (2), 339–366. doi:10.1007/s11242-023-02011-6

Navarrete, I., Lopez, M., and Kurama, Y. (2021). Multi-layer casting of self-consolidating concrete: influence of mortar rheology and casting parameters on the inter-layer bond strength. *Constr. Build. Mater.* 303, 124492. doi:10.1016/j.conbuildmat.2021.124492

Nie, Q., Hu, W., Huang, B., Xiang, S., and He, Q. (2019). Synergistic utilization of red mud for flue-gas desulfurization and fly ash-based geopolymer preparation. *J. Hazard. Mater.* 369, 503–511. doi:10.1016/j.jhazmat.2019.02.059

Othman, O. M., Kchakech, B., Lavaud, S., and Bruno, G. (2016). A new model for the analysis of the structural/mechanical performance of concrete structures affected by DEF–Case study of an existing viaduct. *Struct. Concr.* 17 (6), 1104–1113. doi:10.1002/suco.201500181

Panda, B., Mohamed, N. A. N., Paul, S. C., Singh, G. V. P. B., Tan, M. J., and Šavija, B. (2019). The effect of material fresh properties and process parameters on buildability and interlayer adhesion of 3D printed concrete. *Materials* 12 (13), 2149. doi:10.3390/ma12132149

Qilong Li Birong, YONG, and Guoliang, ZHANG (1999). Review on the development, preparation method and application prospect of functional gradient materials. *J. Yunnan Univ. Technol.* (04), 56–58.

Qinghua, L. I., and Shilong, X. U. (2009). Experimental study on the bending performance of gradient composite beams with crack-control function in ultra-high toughness composites. *Sci. Sin.* 39 (08), 1391–1406. doi:10.1007/s11431-009-0161-x

Tang, Y., Feng, W., Chen, Z., Mai, J., Zheng, J., and Yang, Y. (2024). Behaviour of steel-reinforced recycled aggregate concrete-filled GFRP tubular short columns under eccentric axial compression. *Thin-Walled Struct.* 199, 111818. doi:10.1016/j.tws.2024.111818

Ting, M. Z. Y., Wong, K. S., Rahman, M. E., and Selowara, J. M. (2021). Deterioration of marine concrete exposed to wetting-drying action. *J. Clean. Prod.* 278, 123383. doi:10.1016/j.jclepro.2020.123383

Torelli, G., Mar Giménez Fernández, and Lees, J. M. (2020). Functionally graded concrete: design objectives, production techniques and analysis methods for layered and continuously graded elements. *Constr. Build. Mater.* 242, 118040. doi:10.1016/j.conbuildmat.2020.118040

Wang, C., Yang, C., Qian, J., Zhong, M., and Shuang, Z. (2012). Exothermic behavior of early volcanic ash reaction between fly ash and slag and its mechanism. *J. Chin. Ceram. Soc.* 40 (07), 1050–1058. doi:10.14062/j.issn.0454-5648.2012.07.007

Wang, J., Fan, Y., Zhu, C., Lu, S., and Liu, J. (2020). Mesoscopic finite element simulation on the interfacial bonding performance of functionally gradient concrete. *ES Mater. and Manuf.* 9 (4), 3–11. doi:10.30919/esmm5f810

Wen, X.-D., Ma, B.-G., Gan, W.-Z., and Xian, Z.-W. (2010). Design and research on gradient structure concrete based on volumetric stabilization. *ACI Mater. J.* 107 (6). doi:10.14359/51664048

Wörner, M., Schmeer, D., Schuler, B., Pfinder, J., Garrecht, H., Oliver, S., et al. (2016). Gradientenbetontechnologie: Von der Mischungsentwicklung über den Bauteilentwurf bis zur automatisierten Herstellung. *Bet. Stahlbetonbau* 111 (12), 794–805. doi:10.1002/best.201600056

Xu, Y., Yuan, Q., Li, Z., Shi, C., Wu, Q., and Huang, Y. (2021). Correlation of interlayer properties and rheological behaviors of 3DPC with various printing time intervals. *Addit. Manuf.* 47, 102327. doi:10.1016/j.addma.2021.102327

Yaman, I. O., Hearn, N., and Aktan, H. M. (2002). Active and non-active porosity in concrete part I: experimental evidence. *Mater. Struct.* 35, 102–109. doi:10.1007/bf02482109

Yang Jiujun, J. I. A. X., Tan, W., Guan, Z., and Hairan, W. U. K. (2001). Preliminary study on the physical and mechanical properties of cement-based gradient composite functional materials. *New Build. Mater.* (11), 1–3.

Zhi-Hua, L. I., Qi-Fei, C. U. I., and Kai-Long, S. H. I. (2016). Experimental study on bonding performance of interlayer interface of functional gradient concrete. *Concrete* (11), 16–20. doi:10.3969/j.issn.1002-3550.2016.11.005

Zhouping, Yu, and Yang, W. (2021). Effect of metakaolin on frost resistance and fine structure of vitrified concrete. *J. Funct. Materials/Gongneng Cailiao* 52 (12). doi:10.3969/j.issn.1001-9731.2021.12.031

ZiYu, T. (2023). Study on the deterioration of the performance of finishing ultra-high performance gradient concrete under the compound effect of acid rain carbonation.